Ferroelectrics

ISSN: 0015-0193 (Print) 1563-5112 (Online) Journal homepage: https://www.tandfonline.com/loi/gfer20

An investigation on the growth and propitiates of KDP admixtured ADP single crystals

Iyappan G, Rajesh Paulraj, Ramasamy Perumalsamy, Kamalesh Kumar Maurya & Soma Venugopal Rao

To cite this article: Iyappan G, Rajesh Paulraj, Ramasamy Perumalsamy, Kamalesh Kumar Maurya & Soma Venugopal Rao (2019) An investigation on the growth and propitiates of KDP admixtured ADP single crystals, Ferroelectrics, 550:1, 151-172, DOI: 10.1080/00150193.2019.1652505

To link to this article: https://doi.org/10.1080/00150193.2019.1652505

Published online: 31 Oct 2019.

FERROELECTRICS
2019, VOL. 550, 151–172
https://doi.org/10.1080/00150193.2019.1652505

Taylor & Francis
Taylor & Francis Group

An investigation on the growth and propitiates of KDP admixtured ADP single crystals

Iyappan G[a], Rajesh Paulraj[a], Ramasamy Perumalsamy[a], Kamalesh Kumar Maurya[b], and Soma Venugopal Rao[c]

[a]Department of Physics, SSN Research Centre, SSN College of Engineering, Kalavakkam, Tamil Nadu, India; [b]CSIR–National Physical Laboratory, New Delhi, India; [c]Advanced Centre of Research in High Energy Materials (ACRHEM), University of Hyderabad, Hyderabad, Telangana, India

ABSTRACT

ADP:KDP (85:15) mixed crystal was grown using slow cooling technique. The crystalline perfection of the grown crystal was studied using HRXRD curve. The homogeneity of KDP along the length of mixed crystal was analysed. Low Urbach energy value of the grown crystal indicates good crystallinity of the mixed crystals. Etch pit density was found using chemical etching studies. Vickers hardness studies indicate that the quality of the mixed crystal is more stable compared to ADP. The photoconductive nature and piezoelectric coefficient of the crystal were found. The laser stability of the crystal was observed at 532 nm using Nd:YAG laser.

HIGHLIGHTS

1. Mixed crystal of AKDP in the ratio of 85:15 was successfully grown using slow cooling technique with a size of $45 \times 10 \times 10\,mm^3$
2. Homogeneity of mixed crystal along the entire length of crystal was analysed
3. The band tail energy (Urbach Energy E_U) of the grown crystal was $E_U = 0.91eV$.
4. The calculated etch-pit density for the mixed crystal was $3.6 \times 10^3/cm^2$
5. The piezoelectric charge d_{33} value obtained for the mixed crystal was 6 pC/N.

ARTICLE HISTORY
Received 15 April 2019
Accepted 31 July 2019

KEYWORDS
ADP-KDP; mixed crystal; optical properties; photoconductivity; piezoelectric materials

CONTACT Rajesh P rajeshp@ssn.edu.in Department of Physics, SSN Research Centre, SSN College of Engineering, Kalavakkam, Tamil Nadu, 603110, India
Color versions of one or more of the figures in the article can be found online at www.tandfonline.com/gfer.

GRAPHICAL ABSTRACT

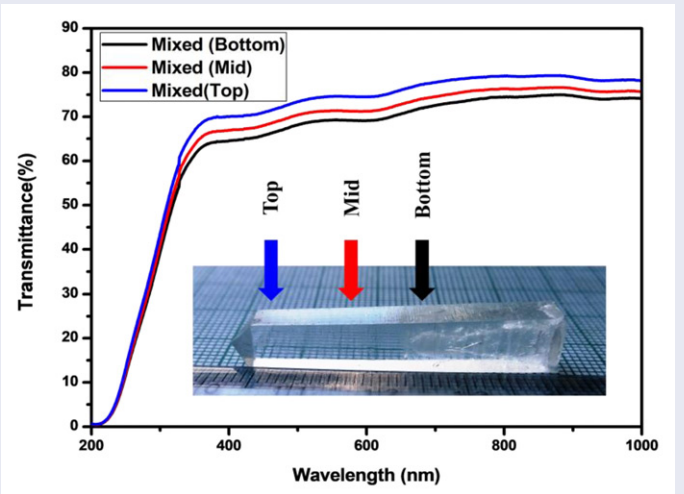

UV- vis spectra for different places, chosen from top to bottom

1. Introduction

Ammonium Dihydrogen Phosphate (ADP) and Potassium Dihydrogen Phosphate (KDP) are used as the second, third and fourth harmonic generator of Nd:YAG and Nd:YLF lasers. Both the materials can be used for electro-optical applications like Q-switch (for Nd:YLF, Nd:YAG lasers) and Ti-sapphire lasers. ADP and KDP shows optical transparency in the wide region of the optical spectrum, high nonlinear efficiency combined with reproducible growth to bulk size and damage resistance to laser radiation. Because of these mentioned properties, the ADP and KDP crystals are extensively used in applications such as nonlinear optical (NLO), electro-optical and photorefractive storage devices [1–4]. Both these materials' growth characteristics have been extensively studied as they can be used to grow bulk size single crystal. The electro-optical, electrical and optical properties of the mixed crystals depend on the parameters like structure, purity, surface, chemical composition interface morphology and homogeneity [3]. In this regard, mixed crystals have been under the focus of researchers due to their unique physical properties which include spin glass state emergence and the anomalous protonic conductivity in a certain intermediate mixing concentration range caused by the competition of antiferroelectric and ferroelectric interactions [5, 6]. S. Sen Gupta *et al.*, reported the physical properties such as lattice parameter and dielectric measurements on KDP and ADP mixed crystal [7]. Ravi *et al.*, have discussed about the structural, mechanical, electrical and optical properties of L-arginine phosphate sulphate (LAPS) and L-arginine Phosphate (LAP) mixed with ADP and KDP Crystals [8]. Rajesh *et al.*, have reported bulk size mixed crystal in the ratio of ADP:KDP (90:10) and compared their properties with pure crystals [6]. Inspite of the extensive research in this area, the growth of defect less bulk size mixed crystals is a great challenge. There

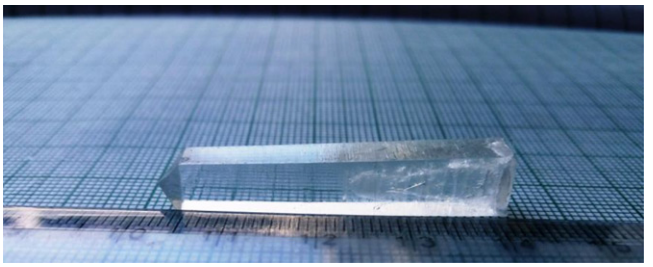

Figure 1. The grown ADP-KDP mixed crystal.

are several problems associated with the growth of such mixed crystals by the conventional slow evaporation technique primarily due to low growth rates and longer periods of growth. Also, this technique is unstable because of spontaneous nucleation from solutions at the high supersaturations which is the primary factor to obtain bulk size crystal with higher growth rates [9–12]. The present work explains the growth and various properties of bulk size AKDP (ADP:KDP) crystal grown with 85:15 composition using slow cooling method. The optical conductivity, extinction coefficient, refractive index, reflectance, Urbach's parameters, work hardening coefficient, yield strength, were calculated.

2. Crystal growth

The ADP and KDP materials were recrystallized four times for purification. The recrystallized material was dissolved in deionised water (resistivity $-18.2\text{M}\Omega$ cm) at room temperature to grow good quality seed crystals. Using slow cooling method, large size crystals were grown from the collected seed crystals. The mounting of the collected seed crystal is done at the platform centre made of acrylic material and is fixed in the crystallizer. The seed mounted platform stirs the solution to avoid stagnant regions. This prevents crystal inclusions which is formed due to solution's supersaturation inhomogeneity. A 5000 ml standard crystallizer is used for the growth of the crystal. An external water bath is used to control the crystallizer temperature. A temperature fluctuation lower than 0.01 K was maintained. The solution filtration was done using 11μm pore sized Whatman filter paper. Next, the filtered solution was heated over to 60 °C for 3 hours and further heat reduced to saturation temperature 50 °C. Then, an ADP crystal of $6\times6\times8\,\text{mm}^3$ size is fixed at crystallizer centre and placed inside the constant temperature bath. The temperature was decreased at a rate of 0.04 °C h^{-1} from the saturation point (50 °C) with a stirring rotation rate of 20 rpm. This was maintained for 25 days. The crystal with a size of approximately $45\text{x}10\text{x}10\,\text{mm}^3$ was harvested (Figure 1).

3. Results and discussion

3.1. Energy dispersive X-Ray analysis (EDX)

The EDX spectrum of AKDP mixed crystal depicted in Figure 2 reveals the presence of K, O, and P. It is inferred that the atomic percentage of O, P and K are 75.7, 21.3 and 3.0 which is very close to the ADP-KDP composition.

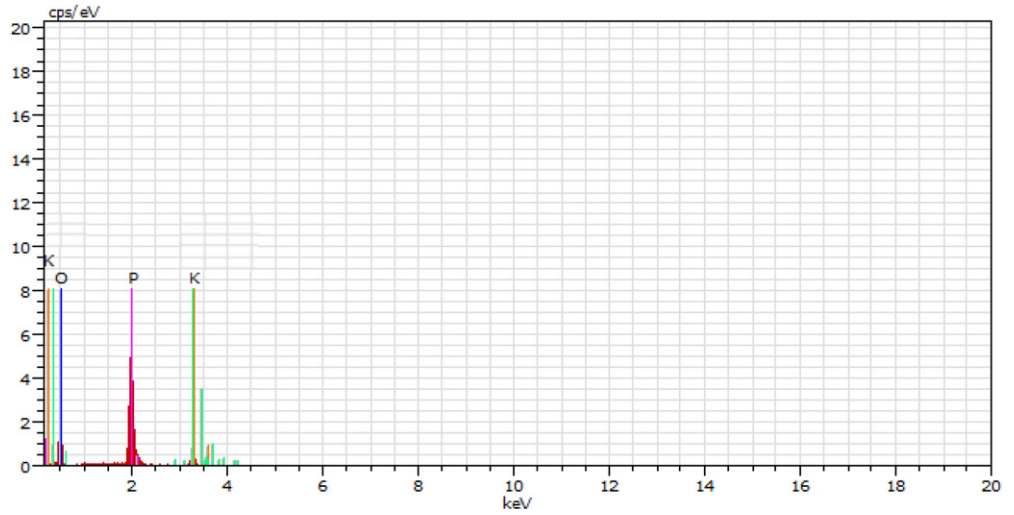

Figure 2. EDAX spectra of grown crystal.

3.2. High resolution X-Ray diffractometry analysis

The Crystalline perfection of AKDP mixed crystal was analysed using High resolution X-ray Diffraction (HRXRD, Panalytical X' Pert PRO MRD system) using CuKα radiation ($\lambda = 1.5405$ Å). The DC (diffraction curve) was recorded using ω scan where the detector was kept at the $2\Theta_B$ angular position with wide opening for its slit. The specimen was chemically etched in a non-preferential mixture of etchant water and acetone at a volume ratio of 1:2 before recording the diffraction curve. This etching removes the undesirable non-crystallized solute atoms that remain on the surface of the crystal and also ensure the surface planarity. Figure 3 depicts diffraction curve recorded for the grown mixed crystal using (200) diffracting planes in symmetrical Bragg geometry using HRXRD. The calculated full width at half maximum (FWHM) is 27 arc s with a very sharp curve satisfying the plane wave dynamical theory of X-ray diffraction [13]. A very sharp DC and absence of additional peaks infers perfect crystallinity of the grown mixed crystal without internal structural grain boundaries [14, 15]. A low value of FWHM indicates the presence of low concentration of unavoidable point defects like self-interstitials and vacancy defects [16, 17]. The decrease in lattice parameter d (interplanar spacing) results in more scattered (also known as diffuse X-ray scattering) intensity at slightly higher Bragg angles (Θ_B) as equation ($2d \sin \Theta_B = n\lambda$; n and λ are the order of reflection and wavelength respectively, which are fixed). The density of such interstitial defect's density is very less which are unavoidable due to thermodynamical conditions. These defects therefore very hardly influence the device performance.

3.3. Optical measurements

3.3.1. Optical transmission and homogeneity analysis of AKDP mixed crystal

The mixed crystal's linear optical property was analysed using Perkin Elmer Lambda-35 UV-Vis-NIR spectrometer in 200–1100 nm range covering the entire visible, near-ultraviolet and

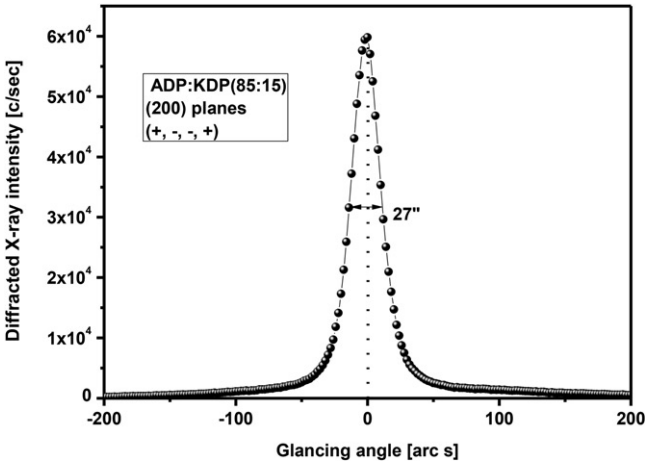

Figure 3. The high-resolution rocking/diffraction curve (DC) recorded for AKDP specimen using (200) diffracting planes.

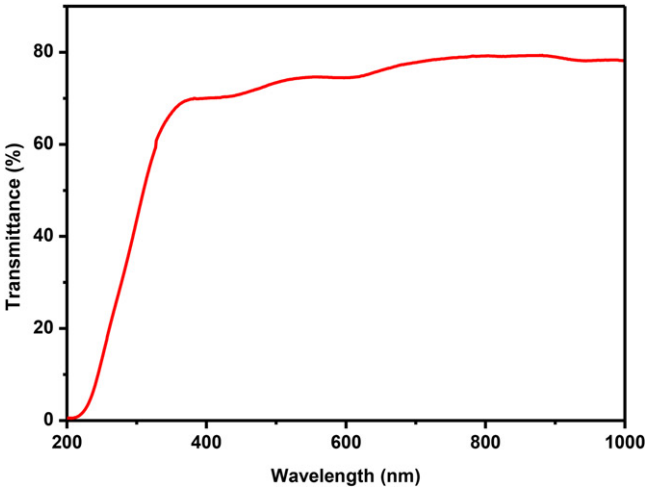

Figure 4. Uv-vis. spectra of grown crystal.

higher energy part of the near-infrared region to find the transmission range. An optically polished 3mm thick mixed crystal was used for this study. The crystal was found to be highly transparent between 350 and 1100 nm (Figure 4). This supports its usage for optical applications. Homogeneity of KDP along the length of crystal was determined by taking the UV-Vis spectra for different places, chosen from bottom to top of the crystal. The transmission spectra were recorded for the different places with uniform thickness. The observed results are shown in Figure 5. The transmission recorded at all these regions (Bottom, Mid and Top) are almost same. To confirm the reproducibility, the beam was passed through the crystal's multiple times and the same spectra were observed. This shows that the KDP is uniformly distributed throughout the crystal. The direct band gap energy was calculated by using the formula as shown below,

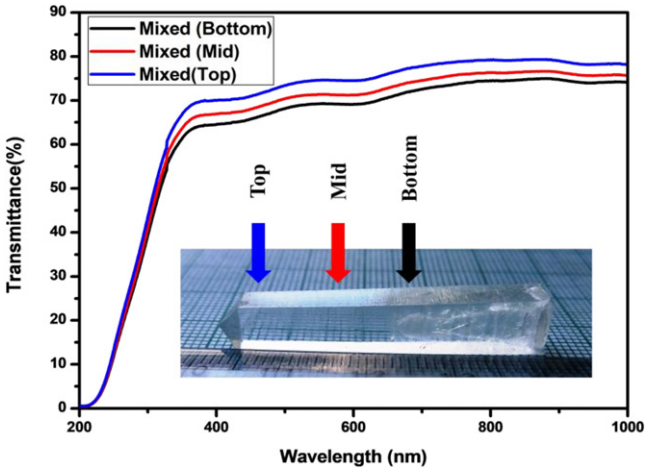

Figure 5. UV-vis spectra for different places, chosen from top to bottom.

$$\alpha h\nu = A(h\nu - E_g)^{\frac{1}{2}}, \tag{1}$$

$$\alpha = \frac{2.3026}{t} log_{10}\left(\frac{100}{T}\right) \tag{2}$$

where E_g is the crystal's optical band gap, A is the constant and ν is the incident light frequency, T is the Transmittance in % and t is the thickness of the grown mixed crystal [18, 19]. The direct optical band gap of the grown mixed crystal is calculated by plotting $(\alpha h\nu)^2$ versus $(h\nu)$. Figure 6 shows the Tauc plot value of grown mixed crystals. The calculated direct optical band gap of the mixed crystal is 4.9 eV.

3.3.2. Determination of optical constants

Proper analysis of optical parameters of mixed crystal provides clear idea about the resolution tuning of various technical devices. The optical conductivity (3), extinction coefficient (4), refractive index (5) and reflectance (6) have been calculated using the transmittance data using following formula [18]

$$\sigma_{op} = \alpha nc/4\pi, \tag{3}$$

$$K = \alpha\lambda/4\pi, \tag{4}$$

$$n_0 = -(R+1) \pm 2\frac{\sqrt{R}}{(R-1)}, \tag{5}$$

$$R = \frac{\exp(-\alpha t) \pm \sqrt{\exp(-\alpha t)T - \exp(-3\alpha t)T + \exp(-2\alpha t)T^2}}{\exp(-\alpha t) + \exp(-2\alpha t)T}. \tag{6}$$

The response of optical conductivity and variation of extinction coefficient with reference to wavelength is shown in Figure 7(a) and (b) respectively. The variation of refractive index and reflectance as a function of wavelength is shown in Figure 8(a) and (b). From the figure, it is noted that the reflectance and refractive index of mixed crystal grown is low in the entire visible region and decreases when compared to pure KDP and ADP crystals. The lower values of extinction coefficient and also higher optical conductivity of mixed crystal in entire

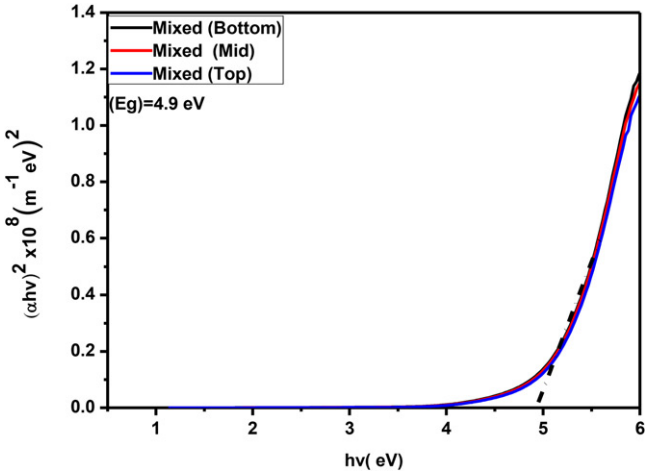

Figure 6. Optical band gap spectrum.

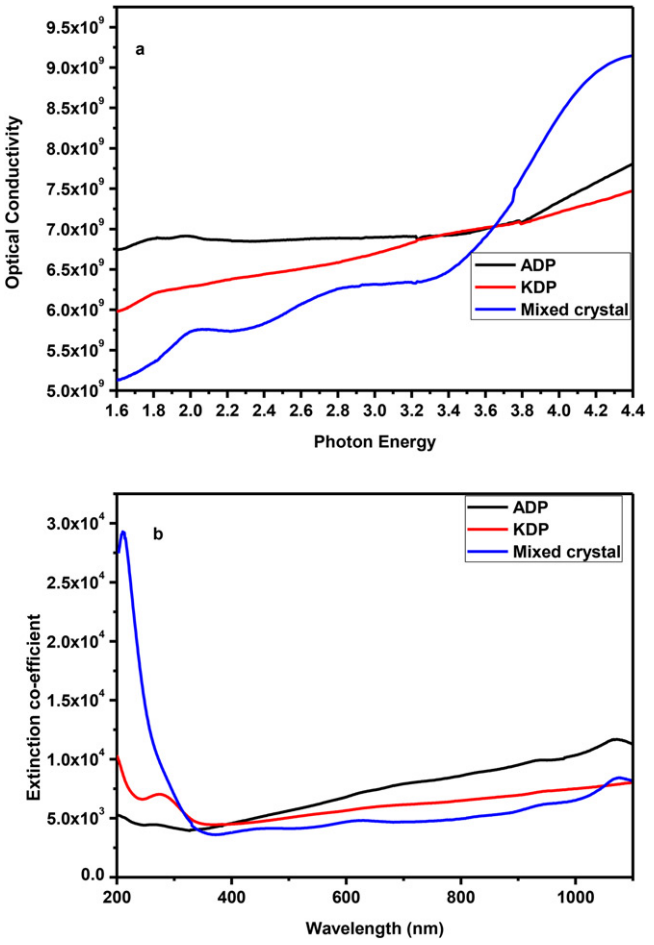

Figure 7. (a) Wavelength dependence of the optical conductivity and (b) Wavelength dependence of the extinction coefficient.

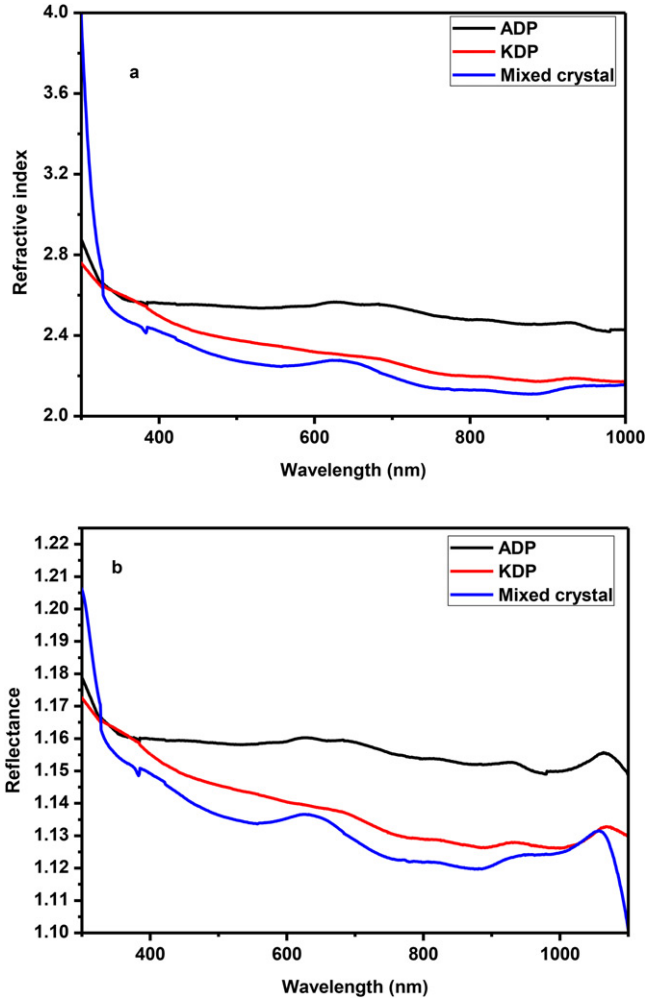

Figure 8. (a) Wavelength dependence of the refractive index and (b) Wavelength dependence of the reflectance.

Table 1. Optical parameters.

Parameter	ADP	KDP	Mixed crystal
Cutoff wavelength	below 200 nm [6]	below 200 nm [6]	210 nm
Bandgap	4.12 ev [22]	4.7eV [23]	4.9 ev
Reflectance	1.18	1.17	1.13
Extinction coefficient	5.2×10^{-6}	4.2×10^{-6}	2.7×10^{-5}

visible region substantiates its application for optical fabrication [20, 21]. The optical studies showed good optical behaviour of the mixed crystal for device application. The obtained results are compared with pure ADP and KDP; the values are tabulated in Table 1.

3.3.3. The Urbach energy (absorption band tail)

An optical absorption spectrum of inorganic material provides the basic information regarding the composition and optical band gap [24]. The material's optical absorption

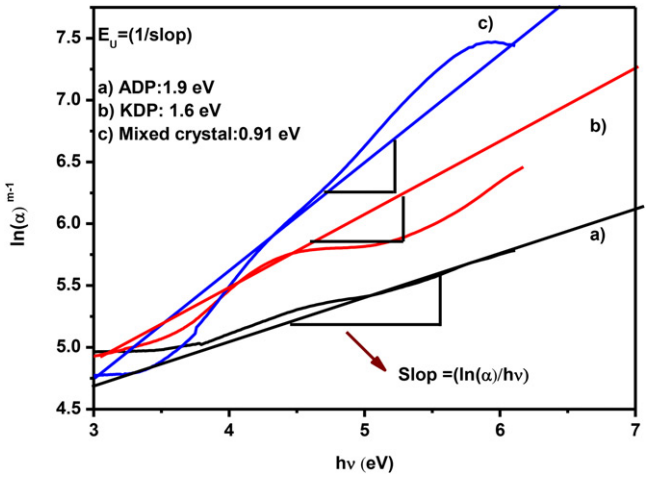

Figure 9. Plot of ln (α) vs. $H\upsilon$.

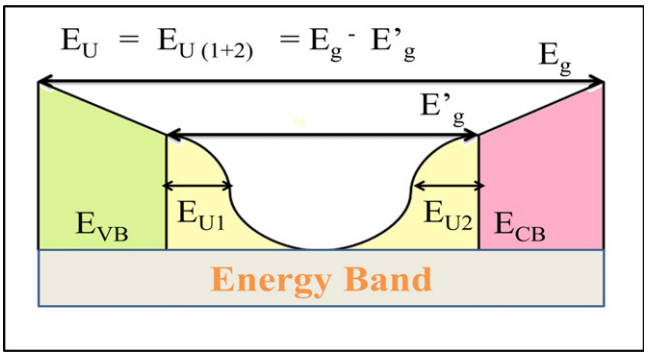

Figure 10. Urbach band tail energy (E_U) diagram.

spectra are of three regions namely weak absorption region due to presence of impurities and defects in the material, absorption edge region because of structural perturbation and system disorder, strong adsorption region which gives the optical band gap energy. The Urbach tail is defined as the exponential part near the optical band edge which is found along the absorption coefficient curve. This appearance of exponential tail in the low crystalline, poorly crystalline, amorphous and disordered materials due to localised states in the band gap extended [22, 25, 26]. The relationship between α and energy of photons ($h\nu$) near the optical band gap edge is called as Urbach empirical rule and is given by the following exponential equation

$$\alpha = \alpha_o \exp\left(h\nu/E_U\right), \tag{7}$$

where, $h\nu$ is the photon energy, α_o is constant and E_U is the Urbach energy (exponential absorption edge width). Straight line equation is obtained by taking the logarithm on both sides of the last equation which is given below.

$$\ln(\alpha) = \ln(\alpha_o) + (h\nu/E_U) \tag{8}$$

Table 2. The obtained Urbach energy (E_U) values for pure and mixed crystal.

Parameter	ADP	KDP	Mixed crystal
Urbach energy (E_U)	3.70 eV	2.44 eV	0.91 eV

From the straight-line slope, the E_U value was calculated (Figure 9). Plotting is done using lnα against the incident photon energy, E. Figure 10 shows the band tail energy diagram. The obtained E_U values are compared with the pure system and tabulated in Table 2. The value of Urbach energy of the grown mixed crystal decreases with the increase in KDP percentage. The band tail broadens along with the disorder increase. This is due to the number of possible bands to tail and tail to tail transitions increase. It was reported that this disorder creates states redistribution and creation of one-to-one tail states at the band states expense [23]. The decrease in the Urbach energy is opposite to the behaviour of the optical energy gap. Good crystallinity and less disorder in the near band edge is the inference from the minimum value of E_U. Another formula that correlates between the absorption coefficient (α) and the optical energy gap [27] suggested by Urbach is shown below.

$$\alpha = \beta \exp\left[\frac{\sigma(h\nu - E_0)}{K_B T}\right] \tag{9}$$

where β is a pre-exponential constant, σ is steepness parameter which is a constant, E_o is the transition energy. E_o is equal to E_g for direct transitions and $E_g \pm E_p$ for indirect transition. Here, E_p is the energy of the phonon associated. For the current crystal sample grown, $E_o = E_g$ which gives the following equation.

$$\ln \alpha = \left(\ln \beta - \frac{\sigma E_g}{K_B T}\right) + \left(\sigma\left(\frac{h\nu}{K_B T}\right)\right) \tag{10}$$

From (8) and (10)

$$\ln \alpha_0 = \left(\ln\beta - \frac{\sigma E_g}{K_B T}\right), \text{ and} \tag{11}$$

$$\frac{(h\nu)}{E_U} = \sigma\left(\frac{h\nu}{K_B T}\right) \tag{12}$$

where, E_U=0.91 eV, K_B is 8.6713×10^{-5} eV/K which is Boltzman constant and T is 273.16 K (Absolute temperature). The steepness parameter σ, is found using Equation 13.

$$\sigma = \left(\frac{K_B T}{E_U}\right) \tag{13}$$

Hence the steepness parameter is calculated either from the slope of Figure 9 or from the Equation (11) directly. The strength of the electron-phonon interaction (E_e–p) is calculated [28–30] from σ using the following equation. The parameters calculated are tabulated and shown in Table 3.

$$E_{e-p} = \frac{2}{3\sigma} \tag{14}$$

Table 3. Steepness parameter (s) and electron phonon interaction (E_{e-p}) of the pure and mixed crystal.

Crystal	The constant (α_0) $\times 10^{-2}$ (cm^{-1})	Steepness parameter (σ) $\times 10^{-2}$	Electrone-phonon interaction $E_{e-p} \times 10^{-2}$
ADP	24	0.63	1.05
KDP	22	0.95	0.70
Mixed crystal	12	2.6	0.25

3.4. Etching analysis

Chemical etching plays influential role in identifying the crystal's growth mechanism and defects. This leads to the improvement of etch spirals, growth striations, step pattern and rectangular etch pits on the surface of the crystal [30]. When the crystal is subjected to any physical or chemical process, these growth units may dissociate themselves from the crystal leaving behind a shallow pit. There are different methods to obtain preferential dissolution on a crystal surface such as 1. thermal etching, 2. chemical etching, 3. electrolytic etching and 4. ionic etching. Chemical etching is the widely adopted method in the field of etching and substantial work on the different crystals is now available in the literature [31, 32]. So, chemical etching study is done using water as an etchant. For the etching times of 5s and 10s, the etching study on the grown mixed crystal was conducted at room temperature to investigate the distribution of structural defects. The grown mixed crystal was dried using tissue papers after dipping in water etchant. Using the reflection mode of optical microscope, the microstructure of the crystals was analysed. A photomicrograph of the grown mixed crystal before etching is shown using Figure 11(a). In this current case, only a few rectangular etch pits which were scattered are observed for the above-mentioned etching time (Figure 11(b) and (c)). It was observed that the size of etch pits enlarged with the etching time increase. The etch-pit density for the mixed crystal calculated is $3.6 \times 10^3/cm^2$. The shape of these etch pits is determined by the lattice structure and symmetry [33]. Also, these etch pits correspond to the dislocation outpoints. The obtained etch pits features show the dislocation position. The presence of dislocations strongly influences many properties of crystal. Also, it is inferred that the crystal does not have layered growth with two-dimensional nucleation mechanism. From these studies, it can be seen that the mixed crystal grown has better quality.

3.5. Microhardness studies

A material's hardness is defined as the measure of resistance when subjected to the local deformation. A selected flat and smooth surface of the mixed crystal grown was subjected to several loads like 5g, 10 g, 25 g, 50 g, 75 g, 100 g at room temperature using Vickers hardness tester fitted with a diamond pyramidal indenter [34]. With constant indentation time of 5s for all the loads, Static indentations were made. Repeated indentations were made at various sites of the grown mixed crystal surface. The Vicker's hardness number was calculated using the relation [35],

$$Hv = 1.8544\left(\frac{P}{d^2}\right)\mathrm{kg/mm^2} \tag{15}$$

where P is the applied load in Kg and d is the indentation impression diagonal length in mm. The Hv, which is the variation of hardness value with the load P and the variation of Hv

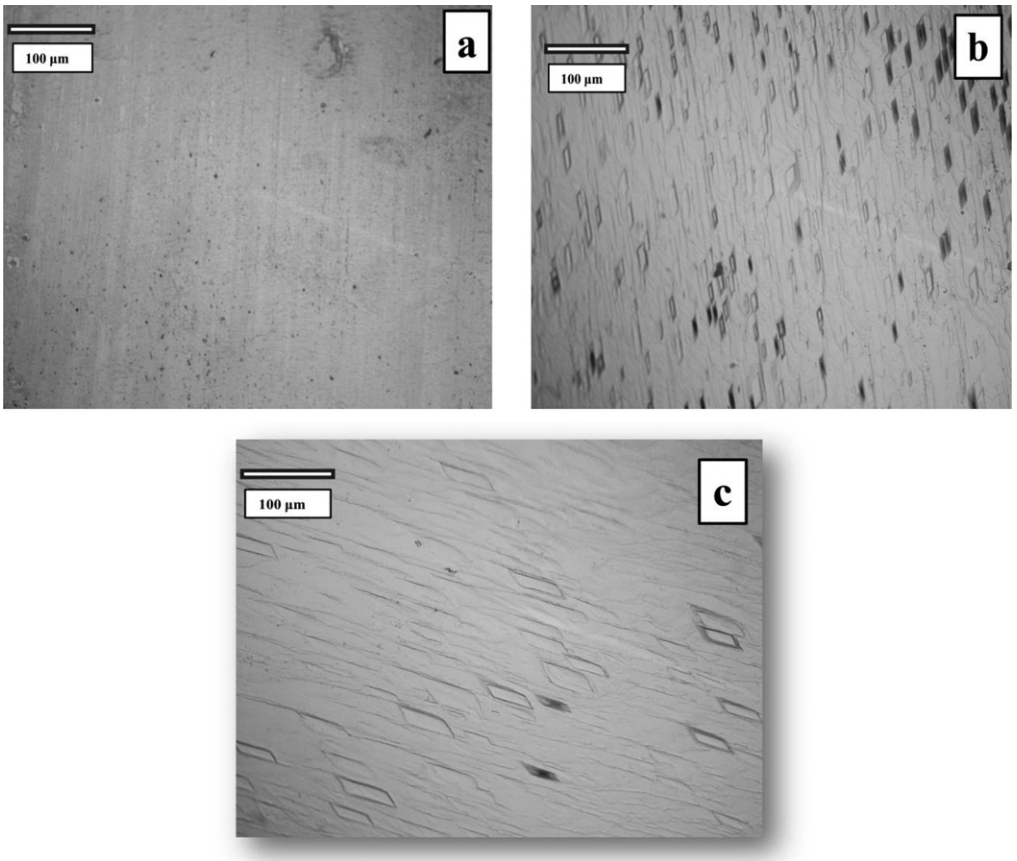

Figure 11. (a) Surface of grown crystal before etching, (b) After water etchant for 5s and (c) after water etchant for 10 s.

against the indentation diagonal d are shown in Figure 12(a) and (b). It shows that the (hv) increases with the increase of applied load (P). It is observed from these results that the hardness increases with the load increase satisfying reverse indentation size effect (RISE) [36].

3.5.1. Analysis of experimental data

The calculation of work hardening coefficient is done from the plot of log P versus log d, the length (l) of radial cracks is related to the function of applied load (P) for indentation by the empirical relation [37].

$$l = C_1 P^{m_1} \tag{16}$$

where C_1 and m_1 are constants. The m_1 value is found and shown in Figure 13 from log l and log p plots. An empirical relation between the length of the crack (l) diagonal of indentation (d) is given by

$$l = C_2 d^{m_2} \tag{17}$$

where, m_2 is found from the $log\ l$ and $log\ d$ plots and is depicted in Figure 14. The work hardening coefficient (n) value is calculated from the below equation with the

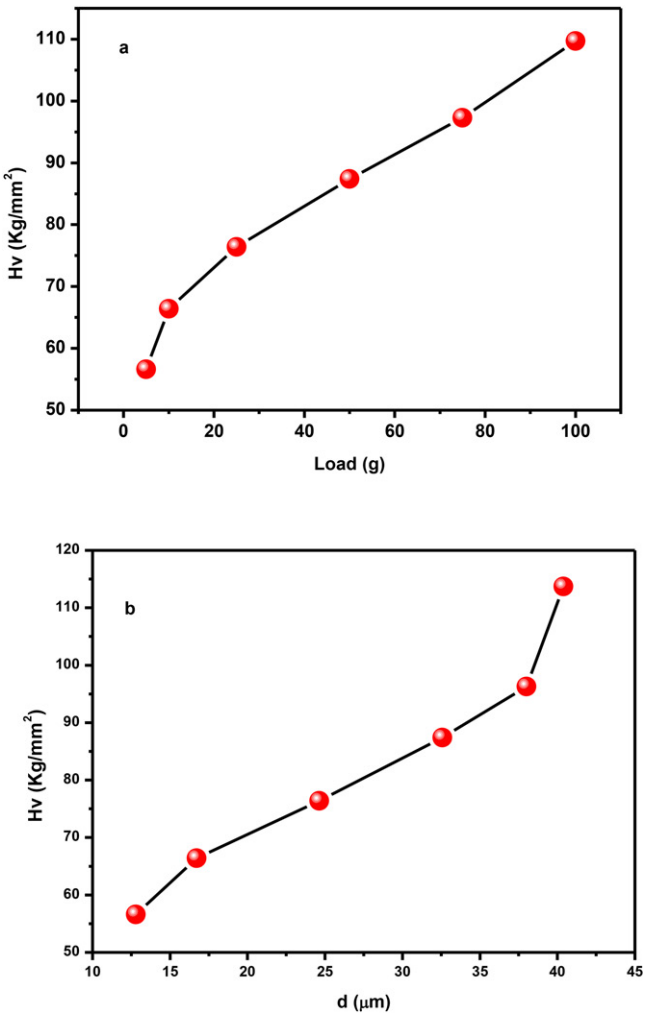

Figure 12. (a) Vikers micro-hardness of grown crystal and (b) Variation of H_v vs diagonal (d).

calculated m_1 and m_2 values where n was found to be 2.38 and which can also be confirmed using Meyer's relation as follows. The Meyer's law (Equation 18) gives the relationship between load and size of the indentation.

$$P = k_1 d^n \tag{18}$$

where k_1 and n are constants for specific material. Figure 15. shows the work hardening coefficient calculated from *log P* versus *log d* plots. After every indentation, material needs time to come back to the elastic mode. Hence a correction x is applied which is known as the dislocation density measure of the material to the d value and related to Kick's law as [38]

$$P = k_2(d + x)^2 \tag{19}$$

From Equations 19 and 20 we have,

$$k_1 d^n = k_2(d + x)^2, \tag{20}$$

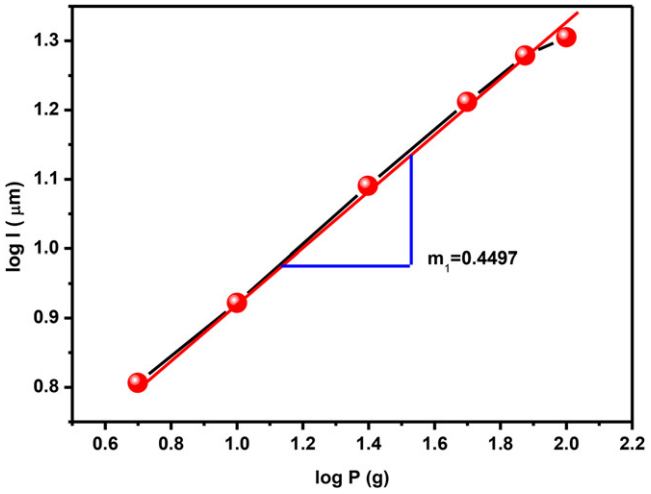

Figure 13. Plot of log I vs log p.

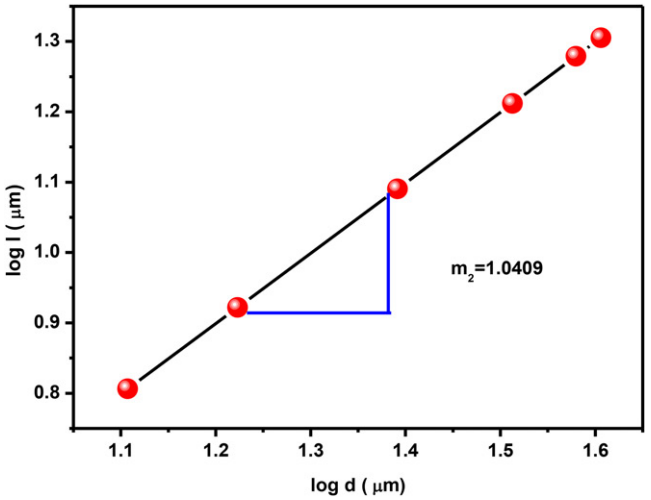

Figure 14. Plot of log I vs log d.

$$(k_1 d^n)^{1/2} = (k_2)^{1/2}(d + x), \tag{21}$$

$$(k_1)^{1/2}(d^n)^{1/2} = (k_2)^{1/2}(d + x), \tag{22}$$

$$\left(\frac{k_1}{k_2}\right)^{1/2} = \frac{d + x}{d^{n/2}}, \tag{23}$$

$$d^{n/2} = \left(\frac{k_2}{k_1}\right)^{1/2} d + \left(\frac{k_2}{k_1}\right)^{1/2} x \tag{24}$$

The slope of $d^{n/2}$ versus d yields $(\frac{k_2}{k_1})^{1/2}$ (Figure 16) and the intercept is a measure of x. The material's yield strength is found using the relation [35]

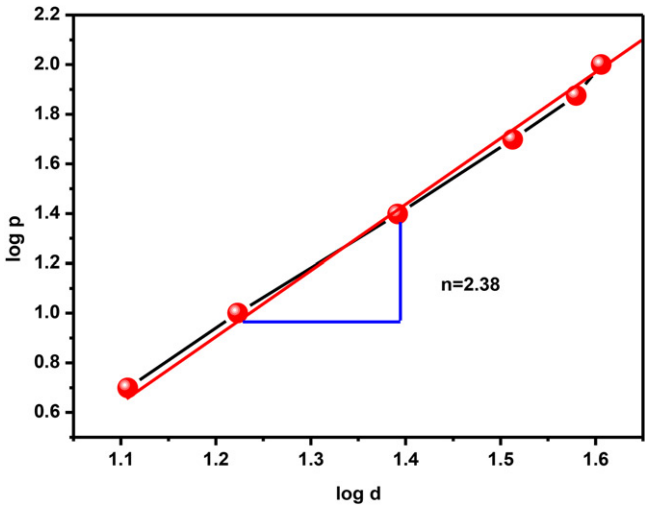

Figure 15. Plot of log P versus log d.

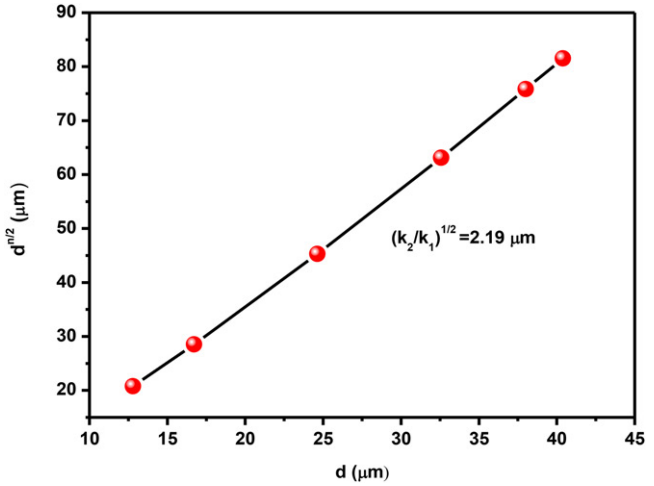

Figure 16. The slope of $d^{n/2}$ versus d.

Table 4. The hardness parameter for the pure and mixed crystal.

Crystal	n	k_1 (10^3 g/μm)	k_2 (g/μm)	X (μm)	σ_ν(MPa)
ADP	1.08	0.97	9.11	0.23	103.17
KDP	2.72	1.01	10.33	0.24	94.23
Mixed crystal	2.38	2.15	5.74	0.25	92.70

$$\sigma_\nu = \frac{Hv}{2.9}\left\{[1-(2-n)] \times \left[\frac{12.5(2-n)}{1-(2-n)}\right]^{n-2}\right\} \tag{25}$$

Using these mentioned relations, the hardness parameter of pure and mixed crystal like x, n, k_1, k_2, σ_ν are calculated and tabulated in Table 4.

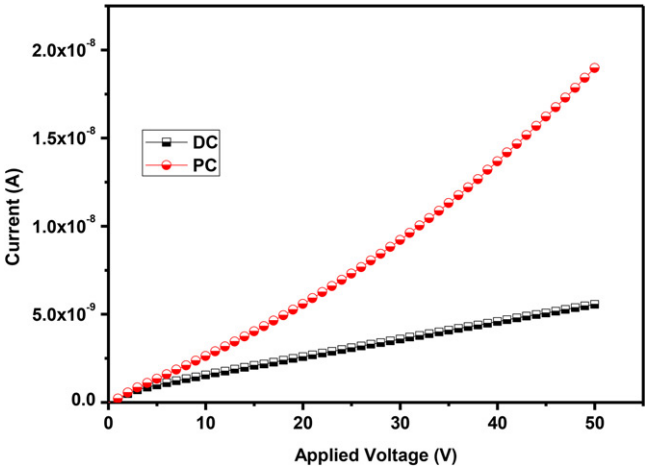

Figure 17. Dark current and photocurrent as function of the applied voltage.

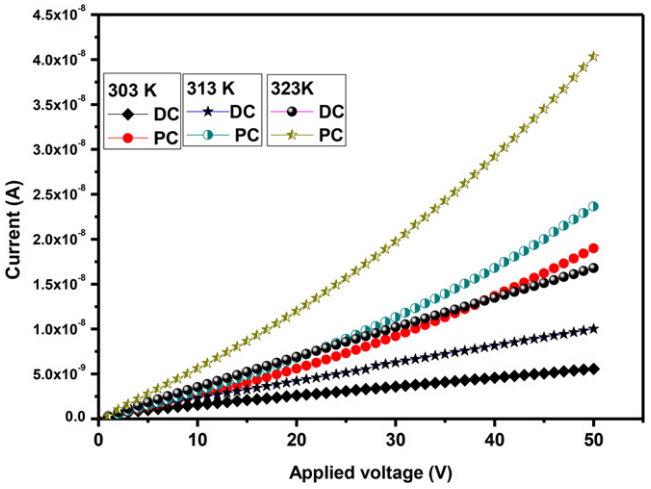

Figure 18. Temperature dependence of Photoconductivity for grown crystal.

3.6. Photoconductivity analysis

The photoconductivity analysis of mixed crystal was done by connecting the crystal sample in series to Kiethley-480 picoammeter and DC power supply. Microprobes were employed as the electrical contacts and connected at 4mm distance of the crystal surface. The applied voltage was in the range of 0 to 50V in steps of 1V/s. To measure the dark current of the mixed crystal, protection from all the possible radiation was done. Then, the crystal sample was exposed to 50 W halogen lamp radiation. The corresponding photocurrent (I_p) is recorded for the same values of the applied voltage. The I_d and I_p nature with the increasing voltage is shown in Figure 17. The linear increase in the dark current and photocurrent with the applied voltage was noted from the photoconductivity study. It is observed that the photocurrent is greater than the dark current and hence the grown mixed crystal has positive photoconductivity. This is due to the increase of charge carriers' numbers or their lifetime in the presence of radiation [39]. Figure 18 shows the distributions of spectra of

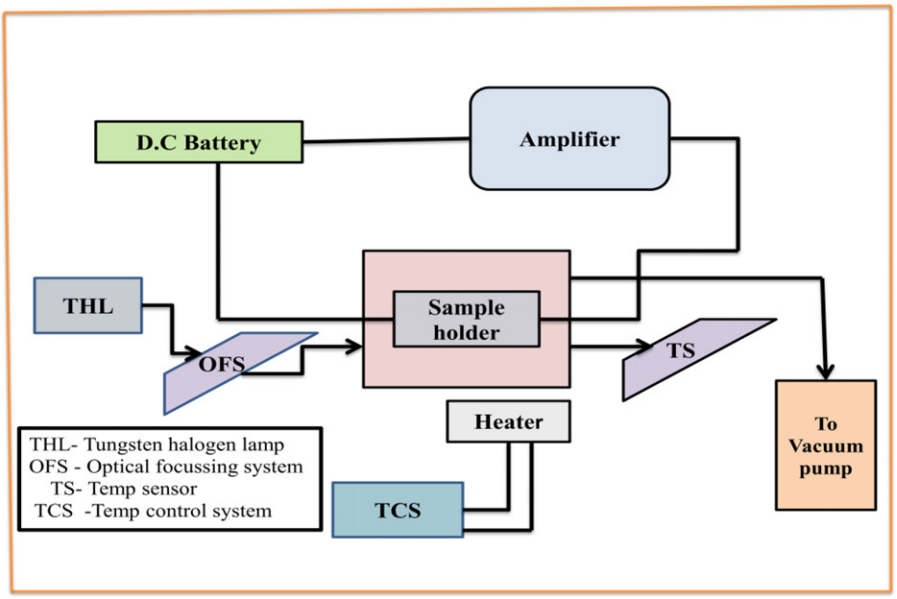

Figure 19. Schematic block diagram of the experimental set-up for the photoconductivity measurement.

Table 5. Piezoelectric coefficient values of the pure and mixed crystal

Crystal	Piezoelectric charge coefficient (d_{33}) value (pC/N)
ADP	2.00
KDP	3.00
Mixed crystal	6.00

DC photocurrent for the grown mixed crystal in the range of 303 K to 323 K. It can be inferred from this figure that the highest value of the photocurrent (Photo-peak) increases as the temperature increases from 303 K to 323 K. This might be due to generation of new charge carriers. The schematic block diagram of the experimental setup for photoconductivity measurement is shown in Figure 19.

3.7. Piezoelectric studies

The lack of centre of symmetry is needed for the existence of useful properties like piezoelectricity in a single crystal. When mechanical force is applied on any piezoelectric materials, they produce electric charge (field) or vice versa [40]. Piezoelectric characterisations is done on the grown mixed crystal. A High-grade silver paste was used to coat the polished basal surface of the crystal. The piezoelectric charge coefficient d_{33} was measured using a piezometer (PM300, Piezo Test, UK). The sample is poled at 205/ kV/cm for 1 hour at room temperature and piezoelectric measurements were carried out. The d_{33} value obtained for the grown mixed crystal was 6 pC/N. This is higher compared to the pure systems. The charge symmetry due to KDP mixing lead to large dipoles when subjected to mechanical stress which briefs the increase of d_{33} value for KDP mixed ADP crystals. These values are shown in Table 5.

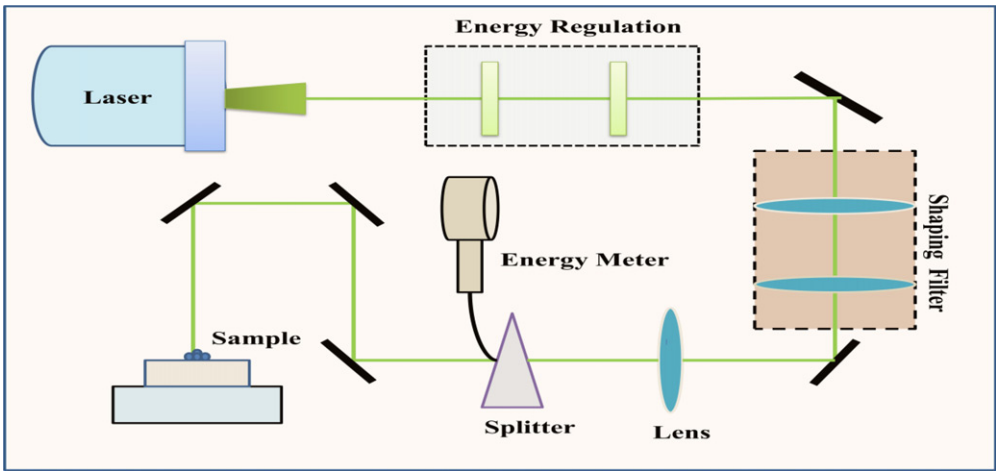

Figure 20. The schematic of the optical layout used for measuring LDT.

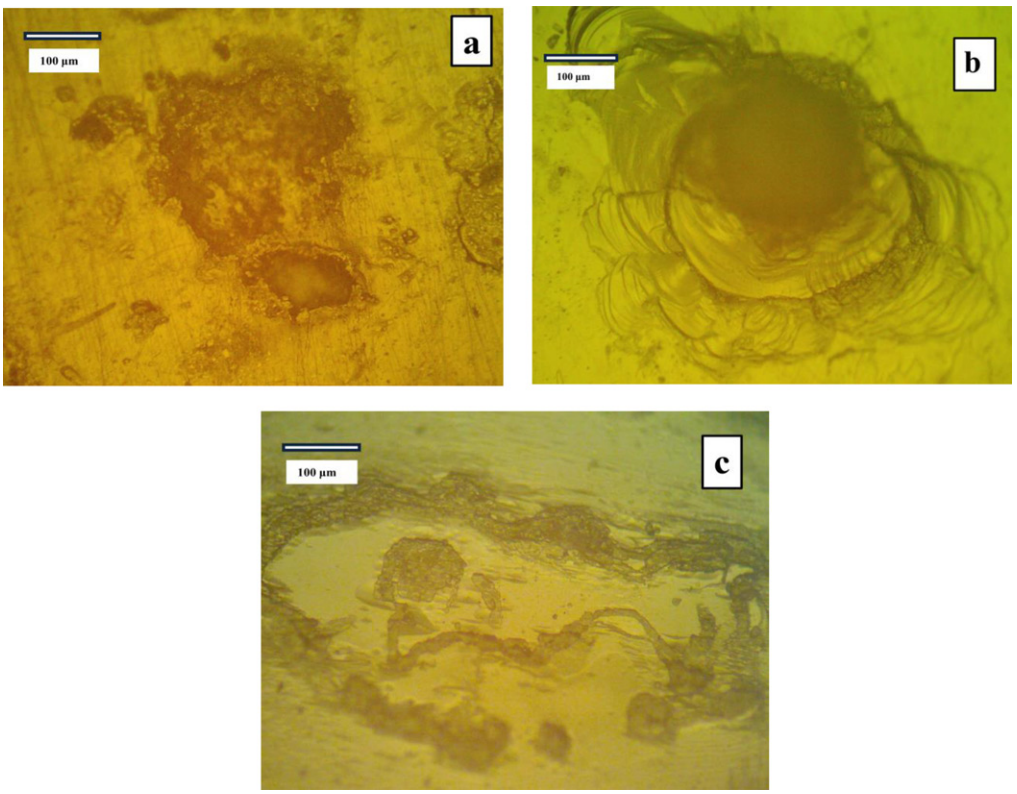

Figure 21. Laser damage profile of a. ADP b. KDP and c. mixed crystal of ADP:KDP (85:15).

3.8. Laser damage studies

Some industries, use frequency converter, buffer ingots or filter of high threshold material to laser damage for laser assisted photonic devices. This increases the durability and efficiency of the fabricated devices. A clear idea of laser damage threshold (LDT) is very important for

Table 6. (a) Laser damage threshold value of ADP, (b). KDP, (c) Mixed crystal AKDP (85:15).

Single shot	
Energy (mJ)	Effects
1	No damage observed
3	No damage observed
5	No damage observed
8	No damage observed
10	A small dot is seen
11	A small dot is seen in the other place
13	Visible crack is seen
15	Heavy damage is seen on crystal surface
Single shot	
Energy (mJ)	**Effects**
1	No damage observed
2	No damage observed
3–5	No damage observed
6	A small dot is seen
7–10	A small dot is seen in the other place
11	A small dot is seen in the other place
12–13	Visible crack is seen
14	Surface damaged
15	Depth crack is seen
16-17	Heavy damage is seen on crystal surface
Single shot	
Energy (mJ)	Effects
1	No damage observed
2	No damage observed
3–5	No damage observed
6	A small dot is seen
7–15	A small dot is seen in the other place
16	Visible damage is seen
17	Small crack is seen
18–20	Surface damaged
25	Depth crack is seen
30	Heavy crack is seen on crystal surface

laser driven devices selectivity [41] as continuous high-power laser exposure, irradiation leads to surface damage. For this investigation, a Q-switched Nd: YAG laser (532 nm, 10 Hz, 7 ns) of pulse mode is configured in order to find the grown crystal's LDT. A 1 mm diameter beam was used to focus on the sample with a 10 cm focal length lens. Figure 20 shows the schematic of the optical layout used for measuring LDT. Both single and multiple shots LDT measurements were made on the samples. The sample is irradiated at different spots on the same plane (100) at similar experimental condition and the damage patterns (Figure 21) were observed using an optical microscope. The detailed data are given in Table 6. The grown mixed crystal's LDT was determined using the following equation

$$P = \frac{E}{\tau \pi r^2} \mathrm{GW/cm^2} \tag{26}$$

where τ is the width of the pulse, E is the energy at which the grown crystal showed damage, and r is the damage spot radius [42]. The damage on the grown crystal due to laser shows the melting, cracks, solidification, fusion or decomposition of the material surface. The LDT of mixed crystal is determined to be 28.3 GW/cm^2. It is clearly evident from table that the damage threshold value of mixed crystal is much higher than pure ADP and KDP crystals (9.8 GW/cm^2 and 10.7 GW/cm^2), which has been determined using the same experimental configurations. This shows the strengthening of

lattice due to KDP molecules interstitial positions on ADP [6]. This analysis proves the mixed crystal's high resistance to optical damage. Hence this mixed crystal grown can be used in the applications related to high power lasers.

4. Conclusions

Good quality mixed crystal of AKDP was successfully grown using slow cooling method. The HRXRD analysis confirms the crystalline perfection of the grown mixed crystal. The transmittance spectrum reveals the transparent nature of the crystal in the entire visible region. Homogeneity of KDP along the length of mixed crystal is found using the UV-Vis spectra for different as-grown regions chosen from top to bottom of the crystal. The optical parameters such as the optical conductivity (σ_{op}), coefficient of absorption (α), reflectance (R), extinction coefficient (K) and refractive index (n) were studied with respect to the wavelengths. Optical studies reveal a shift of the absorption edge toward the higher wavelengths with the addition of KDP. The grown mixed crystal is found to have a lower extinction coefficient, of the order of 10^3. The band tail width (E_U) or Urbach energy is estimated and found to be 0.91 eV. The low value of Urbach energy indicates that the grown mixed crystal has good crystalline perfection. The unambiguous etch pits show good perfection and high quality of the grown mixed crystal. Microhardness test shows the increase of hardness number (H_v) with the increase in load (P). The Meyer index number or work hardening coefficient n was found to be 2.38. Yield strength (σ_v) of the mixed crystal is also analysed and it is found to be 92.7 Mpa. Photoconductivity studies confirm the positive photoconductive characteristics of the mixed crystal at various temperatures. The piezoelectric nature of the mixed crystal has improved when compared with the pure ADP and KDP crystals due to the incorporation of KDP in ADP. The mixed crystal's laser damage threshold is found to be 28.3 GW/cm^2 which is very high than pure ADP and KDP crystal. The higher crystalline perfection, transparency, high mechanical strength, wide band gap, positive photoconductivity, high piezoelectric value and higher laser stability confirm that this mixed crystal grown can be used as a potential material for the optoelectronic devices' fabrication.

Funding

The authors gratefully acknowledge Council of Scientific and Industrial Research (CSIR), Government of India for the financial support [Ref: no. 03 (1362/16/EMR-II].

References

[1] J. Sunil Chaki *et al.*, Synthesis, growth, and characterization of new stilbazolium derivative single crystal: 2-[2-(2,4-dimethoxy-phenyl)-vinyl]-1-ethyl-pyridinium iodide for third-order NLO applications, *Am. J. Phys. Condens. Matter*. **2**, 22 (2012). DOI: 10.5923/j.ajcmp.20120201.0.

[2] J. Podder, S. Ramalingam, and S. narayanakalkura, An investigation on the lattice distortion in urea and KCl Doped KDP single crystals by X-ray diffraction studies, *Cryst. Res. Technol.* **36**(6), 549 (2001). DOI: 10.1002/1521-4079.

[3] P. V. Dhanaraj *et al.*, Growth and characterization of KDP crystals with potassium carbonate as additive, *Cryst. Growth*. **310**(24), 5341 (2008). doi:10.1016/j.jcrysgro.2008.09.019.

[4] V. Rajalekshmi, K. U. Madhu, and C. K. Mahadevan, Electrical properties of pure and glycine added KDP-ADP mixed crystals, *Int. J. Innov, Re s. Sci. Eng. Technol.* **5**, 9193 (2016).
[5] Z. De-Gao, H. Lin-Xiang, and H. Wan-Xia, Growth and characterization of $K_{1-x}(NH_4)_xH_2PO_4$ mixed crystals onto z-cut point seeds, *Cryst. Res. Technol.* **44**(9), 925 (2009). DOI: 10.1002/crat.200900331.
[6] P. Rajesh, P. Ramasamy, and G. Bhagavannarayana, Growth of ADP–KDP mixed crystal and its optical, mechanical, dielectric, piezoelectric and laser damage threshold studies, *J. Cryst. Growth*. **362**, 338 (2013). DOI: 10.1016/j.jcrysgro.2011.10.036.
[7] S. Sen Gupta, T. Kar, and S. P. Sen Gupta, Measurements of lattice parameters and ferroelectric phase transitions in some solution-grown K1-x (NH4) xH2PO4 (KDP: ADP) mixed crystals, *Mater. Chem. Phys*. **58**(3), 227 (1999). DOI: 10.1016/S0254-0584(98)00279-X.
[8] U. Ravi *et al.*, Growth and characterization of sulphate mixed L-arginine phosphate and ammonium dihydrogen phosphate/potassium dihydrogen phosphate mixed crystals, *J. Cryst. Growth*. **137**(3–4), 598 (1994). DOI: 10.1016/0022-0248(94)91004-9.
[9] K. Srinivasan, S. Anbukumar, and P. Ramasamy, Mutual solubility and metastable zone width of $NH_4H_2PO_4$—KH_2PO_4 mixed solutions and growth of mixed crystals, *J. Cryst. Growth*. **151**(1–2), 226 (1995). DOI: 10.1016/0022-0248(95)00054-2.
[10] K. Srinivasan *et al.*, Mixed Crystals of NH4H2PO4–KH2PO4: Compositional Dependence of Morphology, Microhardness and Optical Transmittance, *Mater. Sci. Eng.* **52**, 133 (1998).
[11] D. Xu and D. Xue, Chemical bond simulation of KADP single-crystal growth, *J. Cryst. Growth*. **310**, 1385 (2008). DOI: 10.1016/j.jcrysgro.2007.12.008.
[12] N. P. Zaitseva, L. N. Rashkovich, and S. V. Bogatyreva, Stability of KH_2PO_4 and $K(H,D)_2PO_4$ solutions at fast crystal growth rates, *J. Cryst. Growth*. **148**(3), 276 (1995). DOI: 10.1016/0022-0248(94)00606-7.
[13] G. Bhagavannarayana *et al.*, Enhancement of crystalline perfection by organic dopants in ZTS, ADP and KHP crystals as investigated by high-resolution XRD and SEM, *J. Appl. Crystallogr*. **39**(6), 784 (2006). DOI: 10.1107/S0021889810033649.
[14] R. Ramesh Babu *et al.*, Growth, structural, spectral, mechanical and optical properties of pure and metal ions doped sulphamic acid single crystals, *Spectrochim Acta A Mol Biomol Spectrosc*. **76**(5), 470 (2010). DOI: 10.1016/j.saa.2010.04.001.
[15] P. Rajesh, and P. Ramasamy, Effect of oxalic acid on the optical, thermal, dielectric and mechanical behaviour of ADP crystals, *Physica B*. **404**, 611 (2009).
[16] S. Balamurugan, G. Bhagavannarayana, and P. Ramasamy, Growth of unidirectional potassium dihydrogen orthophosphate single crystal by SR method and its characterization, *Mater. Lett*. **62**(24), 3963 (2008). DOI: 10.1016/j.matlet.2008.05.047.
[17] S. Balamurugan *et al.*, Investigation of SR method grown ⟨0 0 1⟩ directed KDP single crystal and its characterization by high-resolution X-ray diffractometry (HRXRD), laser damage threshold, dielectric, thermal analysis, optical and hardness studies, *Mater. Chem. Phys*. **117**, 465 (2009). DOI: 10.1016/j.matchemphys.2009.06.021.
[18] O. Donald Nnanyere, Optical properties of barium sulphide thin films prepared by chemical bath deposition technique, *J. Appl. Phys*. **7**, 10 (2015).
[19] M. Elahi, and D. Souri, Study of optical absorption and optical band gap determination of thin amorphous TeO_2-V_2O_5-MoO_3 blown films, *Indian J. Pure. Ap.phy*. **44**, 468 (2006). Doi: nopr.niscair.res.in/handle/123456789/8324.
[20] T. C. Sabari Girisun, and S. Dhanuskodi, Linear and nonlinear optical properties of tris thiourea zinc sulphate single crystals, *Cryst. Res. Technol*. **44**(12), 1297 (2009). DOI: 10.1002/crat.200900351.
[21] F. Yakuphanoglu, and H. Erten, Frequency independent-dependent conductivity and dielectric properties of some ionomers, *Optic Appl*. **35**, 969 (2005).
[22] K. A. Aly *et al.*, Optical properties of Ge–As–Te thin films, *Physica B*, **406**(22), 4227–4232 (2011). DOI: 10.1016/j.physb.2011.08.013.
[23] K. Stephen *et al.*, Disorder and optical absorption in amorphous silicon and amorphous germanium, *J. Non-Cryst. Solids*. **210**, 249 (1997). DOI: 10.1016/S0022-3093(96)00612-6.

[24] A. S. Hassanien, and Alaa A. Akl, Effect of Se addition on optical and electrical properties of chalcogenide CdSSe thin films, *Superlattice Microst.* **89**, 153 (2016). DOI: 10.1016/j.spmi.2015.10.044.
[25] J. Melsheimer, and D. Ziegler, Band gap energy and Urbach tail studies of amorphous, partially crystalline and polycrystalline tin dioxide, *Thin Solid Films.* **129**(1–2), 35 (1985). DOI: 10.1016/0040-6090(85)90092-6.
[26] S. J. Ikhmayies, and R. N. Ahmad-Bitar, A study of the optical bandgap energy and Urbach tail of spray-deposited CdS: In thin films. *J. Mater. Res. Technol.* **2**(3), 221 (2013). DOI: 10.1016/j.jmrt.2013.02.012.
[27] J. Tauc, *Amorphous and Liquid Semiconductors* (Plenum Press, New York 1974).
[28] M. El-Hagary *et al.*, Effect of γ-irradiation exposure on optical properties of chalcogenide glasses $Se_{70}S_{30-x}Sb_x$ thin films, *Phys. Chem.* **81**, 1572 (2012). DOI: 10.1016/j.radphyschem.2012.05.012.
[29] M. Karimi *et al.*, Retracted: Controlled synthesis, characterization and optical properties of CdS nanocrystalline thin films via chemical bath deposition (CBD) route, *Curr. Appl. Phys.* **9**(6), 1263 (2009). DOI: 10.1016/j.cap.2009.02.006.
[30] G. H. Sun *et al.*, Nucleation kinetics and etching studies of deuterated l-arginine trifluoroacetate crystal, *Chem. Phys.* **122**, 524 (2010). DOI: 10.1016/j.matchemphys.2010.03.038.
[31] B. Vander Hoek, J. P. Eerden, and P. Bennema, The influence of stress on spiral growth, *J. Cryst. Growth.* **58**, 365 (1982). DOI: 10.1016/0022-0248(82)90284-6.
[32] S. Mukerji, and T. Kar, Etch pit study of different crystallographic faces of L-arginine hydrobromide monohydrate (LAHBr) in some organic acids, *J. Cryst. Growth.* **204**(3), 341 (1999). DOI: 10.1016/S0022-0248(99)00137-2.
[33] K. Sangwal, and I. Owczarek, On the formation of etch grooves at impurity striations and growth sector boundaries in crystals grown from solutions, *J. Cryst Growth.* **129**(3–4), 640 (1993). DOI: 10.1016/0022-0248(93)90500-V.
[34] B. W. Mott, *Microindentation Hardness Testing* (Butterworth, London 206; 1956).
[35] P. Rajesh *et al.*, Enhancement of the crystalline perfection of <0 0 1> directed KDP single crystal, *Curr. Appl. Phys.* **11**, 1343 (2011). DOI: 10.1016/j.cap.2011.03.076.
[36] K. Sangwal, On the reverse indentation size effect and microhardness measurement of solids, *Mater. Chem. Phys.* **63**(2), 145 (2000). DOI: 10.1016/S0254-0584(99)00216-3.
[37] S. Dinakaran *et al.*, Growth of a bulk organic single crystal of benzoylglycine by the unidirectional crystal growth method, *Cryst. Growth. Des.* **9**, 1 (2009).
[38] R. H. Bube, *Photoconductivity of Solids* (Wiley, New York 1981).
[39] S. Pandi, and D. Jayaraman, Studies on photoconductivity of C60 and C60-doped poly(vinylchloride), *Mater. Chem. Phys.* **71**, 314 (2001). DOI: 10.1016/S0254-0584(01)00285-1.
[40] H. Nakatani *et al.*, Laser-induced damage in beta-barium metaborate, *Appl. Phys. Lett.* **53**(26), 2587 (1988). DOI: 10.1063/1.100535.
[41] M. I. Baig, M. Anis, and G. G. Muley, Influence of tartaric acid on linear-nonlinear optical and electrical properties of KH2PO4 crystal, *Opt. Mater.* **72**, 1 (2017). DOI: 10.1016/j.optmat.2017.05.042.
[42] K. Nivetha *et al.*, Synthesis, growth, and characterization of new stilbazolium derivative single crystal: 2-[2-(2,4-dimethoxy-phenyl)-vinyl]-1-ethyl-pyridinium iodide for third-order NLO applications, *J. Mater. Sci: Mater. Electron.* **28**(7), 5180 (2017). DOI: 10.1007/s10854-016-6174-x).